Jefferson Lab PAC 34 Proposal

Precise Measurement of π^+/π^- Ratios in Semi–inclusive Deep Inelastic Scattering Part I: Charge Symmetry Violating Quark Distributions

December 15, 2008

J. Arrington, R. Dupré, D. Geesaman, K. Hafidi (spokesperson[1]), R. J. Holt, D. H. Potterveld, P. E. Reimer, P. Solvignon

Argonne National Laboratory, Argonne, IL

W. Chen, H. Gao, X. Qian, Y. Qiang, Q. Ye

Duke University, Durham, NC

P. Markowitz

Florida International University, Miami, FL

C. .E. Keppel

Hampton University, Hampton, VA

G. Niculescu, I. Niculescu

James Madison University, Harrisonburg, VA

P. Bosted, R. Ent, H. Fenker, D. Gaskell (spokesperson), D. Mack, G. Smith

Jefferson Lab, Newport News, VA

J. Dunne, D. Dutta (spokesperson), E. Leggett, A. Narayan, L. Ndukum, Nuruzzaman, A. Subedi

Mississippi State University, Mississippi State, MS

A. Daniel

Ohio University, Athens, OH

E. Beise

University of Maryland, College Park, MD

G. Huber

University of Regina, Regina, SK, Canada

H. Baghdasaryan, D. Day, N. Kalantarians

University of Virginia, Charlottesville, VA

F. .R. Wesselman

Xavier University of Louisiana, New Orleans, LA

[1] Contact person, kawtar@anl.gov

A. Asaturyan, A. Mkrtchyan, H. Mkrtchyan, V. Tadevosyan
Yerevan Physics Institute, Yerevan, Armenia

I. CONTRIBUTION TO THE HALL C 12 GEV UPGRADE

The co-spokespersons for this experiment plan to contribute to the implementation of the Hall C upgrade for 12 GeV in both manpower and materials.

Dipangkar Dutta will help design and commission the collimators and sieve slits for the SHMS spectrometer. He is seeking funding to build a GEM based forward tracker which in combination with the slits and collimators will be used to understand and model the magnetic transport of the spectrometer. He is also seeking funding to build an aerogel Čerenkov counter for the SHMS (not part of baseline equipment). His group will also contribute manpower towards the upgrade and commissioning of the SHMS.

David Gaskell will support the SHMS construction and detector assembly and is responsible for ensuring functionality of the Hall C Møller and Compton polarimeters at 12 GeV. In addition, he will devote time to updating and maintaining the Hall C simulation package SIMC. This will entail, not only incorporating the SHMS into the existing simulation, but helping with spectrometer optics calculations.

Kawtar Hafidi and the Argonne group has been contributing towards the initial optics design of the SHMS. They will also perform optics commissioning and verification of the SHMS.

II. ABSTRACT

We propose to measure precision ratios of charged pion electroproduction in Semi–Inclusive Deep Inelastic Scattering from deuterium. This experiment is Part I of a program of two experiments. In this experiment (Part I), data from the deuterium target alone will be used to test the validity of charge symmetry in the valence quark distributions. In Part II, gold and deuterium data will be combined to test the flavor dependence of the EMC effect in the valence region. The two experiments are proposed together due to the similar technique, i.e. precision measurements of charged pion ratios, and overlap in kinematics.

This experiment will use the SHMS and HMS in Hall C to measure electrons and charged pions in coincidence. In this case, the SHMS will be used as the electron arm, and the HMS as the hadron arm. The experiment will measure semi–inclusive production of charged pions at three different values of Q^2=3.5, 5.1, and 6.1 GeV^2 at large x. A range of x and z values is required to fully contrain charge symmetry violating contributions in both the quark distributions and fragmentation functions.

Charge symmetry in the valence quark distrubtions has never been tested with precision, and if broken could have profound consequences regarding our assumptions about quark distributions at large x. In addition, violation of charge symmetry in quark distributions has consequences reaching beyond QCD and would impact, for example, the recent extraction of the Weinberg angle from neutrino DIS.

This experiment, run alone, requires 17 days to complete in Hall C assuming a maximum of 50 μA beam current and a beam energy of 11 GeV. The majority of the deuterium data needed for Part II is taken at common kinematics with this proposal, so if run together the overhead is reduced. The total time needed to run Part I and Part II run together is 35.5 days.

III. INTRODUCTION

Everybody agrees on the importance of testing fundamental symmetries, even approximate ones. In this proposal we are interested in measuring charge symmetry violation in valence quark distributions. In parton distribution functions, it is routinely assumed that charge symmetry is valid. Surprisingly enough, there are no direct measurements of such a contribution, and this makes these measurements even more important. Measurement of a nonzero effect would be extremely interesting and will have various important implications on recent topics such as the measurement of Weinberg angle using neutrino deep inelastic scattering. Semi-inclusive deep inelastic scattering on deuterium can be used to probe

charge symmetry violation effects. Charged pions will be detected in coincidence with the scattered electrons. Efficient detection of both signs of charged pions is important, but absolute yields are not required as overall normalizations cancel out in the measured ratio.

The organization of this proposal is as follows. In section IV, we discuss the physics motivation and the important implications of these measurements. Section V discusses the validity of factorization assumption for JLab energies. In section VI, we review the formalism for semi-inclusive pion production on deuterium. The experimental details and rates are given in section VII. Different corrections and corresponding systematical errors are discussed in section VIII. The expected precision is presented in IX. Finally, the beam time request is presented in section X.

IV. PHYSICS MOTIVATION

Symmetries are the key to understanding and classifying the structure of matter and the fundamental forces. Their study leads to better understanding of the underlying physics. With the advances in experimental and theoretical tools, symmetries other than those of space-time were introduced in physics. Isospin (IS) and charge (CS) symmetries are examples. They are not exact symmetries in nuclear systems. While IS requires invariance under all rotations in isospin space such that the Hamiltonian of the system commutes with the isospin operator (T), *i.e.*

$$[H, T] = [H, T^2] = 0,$$

CS is related to only one rotation. It requires invriance with respect to rotations of 180^o about the T_2 axis, where the charge corresponds to the third axis. If CS is a valid symmetry the Hamiltonian has to commute with the charge symmetry operator P_{CS}, *i.e.*

$$[\mathrm{H},\, \mathrm{P}_{CS}] = 0, \;\; \text{where} \;\; \mathrm{P}_{CS} = \exp(\mathrm{i}\pi T_2),$$

Consequently, IS implies CS but not the converse. CS is used to understand many relations between strong interaction processes. For details we refer the reader to comprehensive reviews by Miller, Nefkens and Slaus [1], and Henley and Miller [2]. For nuclei, the CS operator interchanges neutrons and protons. Thus, CS implies the equality of the neutron-neutron and proton-proton interaction. Also, it requires that two mirror reactions in isospin space have the same cross section, e.g., $\sigma(\mathrm{n},{}^3\mathrm{He}) = \sigma(\mathrm{p},{}^3\mathrm{H})$. Furthermore, CS predicts the equality of mirror nuclear masses, e.g., $\mathrm{m}({}^3\mathrm{He}) = \mathrm{m}({}^3\mathrm{H})$, and it establishes relationships between spin and polarization observables.

At the quark level, P_{CS} acts only on the two light quark flavors:

$$P_{CS} \mid d \rangle = \mid u \rangle \text{ and } P_{CS} \mid u \rangle = - \mid d \rangle,$$

CS implies the invariance of a system under the interchange of up and down quarks while simultaneously interchanging protons and neutrons, *i.e.*

$$u^p(x, Q^2) = d^n(x, Q^2)$$

$$d^p(x, Q^2) = u^n(x, Q^2)$$

Quantum Chromo-Dynamics (QCD) provides a clear formulation of the origin of charge symmetry violation (CSV). In QCD, the only sources of CSV are electromagnetic interactions and the mass difference $\delta m = m_d - m_u$ between down and up quarks. Electromagnetic interactions should play a minor role at high energies. Thus, the light quark mass difference is the interesting feature of the QCD view of CSV [3].

CS is a more restricted symmetry than IS; therefore it is generally conserved in strong interactions to a greater degree than IS. Isospin violating forces produce large differences betwen nn and np scattering lengths and effective ranges in the $^1S_0$ state. The effect of isospin violating forces is large at low energies because the $^1S_0$ state is almost bound. Charge symmetry appears to be more respected than isospin symmetry [2]. The difference between nn and pp (after correction for direct electromagnetic effects) scattering lengths is small or zero; the difference in the corresponding effective ranges is hard to determine. Thus, while in many nuclear reactions IS is violated at the few percent level, in most cases CS is obeyed to better than one percent: the proton and neutron masses are equal to about 1%; the binding energies of tritium and ^{3}He are equal to 1%, after Coulomb corrections. By comparing energy levels in mirror nuclei, one generally finds agreement to better than 1%, after correcting for electromagnetic interactions. At the parton level, one would naively expect CSV to be of the order of the up-down current quark mass difference divided by some average mass expectation value of the strong Hamiltonian, *i.e.*, $(m_d - m_u)/ < M >$, where $< M >$ has a value roughly 0.5-1.0 GeV. This would put CSV effects at a level of 1% or smaller [4].

From our experience with CS in nuclear systems, and because of the order of magnitudes estimates of CSV in parton systems, CS has been universally assumed in quark distribution functions. It is so common in quark-parton phenomenology that it is frequently not even mentioned as an assumption. CS reduces by a factor of two the number of independent quark distributions necessary to describe high energy data, and until recently there has been no compelling reason to suggest CSV. On the other hand, there were no precise tests of charge symmetry in parton distributions. Recently much attention has been focused on the apparent violation of what is called SU(2) flavor symmetry in the nucleon. This was suggested by New Muon Collaboration (NMC) [5] and later supported by results from NA51

group at CERN [6] and E866 Drell-Yan experiment [7] at FNAL. Experimental results from these collaborations seem to show a large flavor symmetry violation in the proton sea quark distributions (i.e. $\bar{u}^p(x) \neq \bar{d}^p(x)$). However this could also in principle be explained even if flavor symmetry were conserved, if we assume CSV in the nucleon sea. The valence quark CSV is also a very important issue because it makes a substantially larger contribution than the sea quark CSV to the extraction of the Weinberg angle from neutrino Deep Inelastic Scattering (DIS). The three standard deviation result from the Standard Model prediction reported by NuTeV collaboration [8] or the so called "NuTeV anomaly" could be completely removed by assuming valence quark CSV.

In this proposal, we are interested in CSV in valence quark distributions. At present, there are no direct measurements that reveal the presence of CSV in parton distribution functions. We have only upper limits on the magnitude of CSV. These limits arise from comparing the structure function F_2^ν measured in neutrino induced charged current reactions, and the structure function F_2^γ for charged lepton DIS, both measurements on isoscalar targets [9]. The most precise neutrino measurements were obtained by the CCFR collaboration [12], who extracted the F_2^ν structure function for neutrino and anti-neutrino interactions on iron at FNAL. The NMC collaboration performed the most precise measurements of F_2^γ structure functions using muon interaction on deuterium at E_μ = 90 and 280 GeV. In the region of $0.1 \leq x \leq 0.4$, an upper limit of 9% was set for CSV effects.

Several theoretical investigations of CSV in valence quark distributions have been carried out initially by Sather [13] and by Rodionov et al [14]. They calculated valence quark distributions for the proton and neutron in a quark model and in the MIT bag model, respectively. In both models, $u^p(x)$ and $d^n(x)$ satisfied CS to within 1% while $d^p(x)$ and $u^n(x)$ were predicted to violate charge symmetry by 5% or more at large x values. In addition, both calculations predict opposite signs for $\delta u_v = u_v^p(x) - d_v^n(x)$ and $\delta d_v = d_v^p(x) - u_v^n(x)$ in the valence region.

Because theoretical estimates put parton CSV at the percent level and because of the lack of direct evidence for violation of parton charge symmetry, all previous phenomenological parton distribution functions have assumed the validity of parton charge symmetry. However, the MRST group [15] has recently studied the uncertainties in parton distribution functions (PDFs) arising from a number of factors, including charge symmetry violation. They constructed a functional form for CSV component that automatically satisfied the quark normalization condition:

$$\int_0^1 dx \delta d_v(x) = \int_0^1 dx \delta u_v(x) = 0$$

where $\delta u_v(x) = -\delta d_v(x) = \kappa f(x)$. This function has the following form:

$$f(x) = (1-x)^4 x^{-0.5}(x - 0.0909)$$

The function $f(x)$ was chosen so that at both small and large x, $f(x)$ has the same form as the MRST valence quark distributions and the first moment of $f(x)$ is zero. The functional form of the valence CSV distributions guaranteed that δu_v and δd_v would have opposite signs at large x, in agreement with the theoretical calculations mentioned previously. The overall coefficient κ was then varied in a global fit to a wide range of high energy data. The value of κ which minimized χ^2 was $\kappa = -0.2$. The MRST distribution of χ^2 vs. κ has a shallow minimum with 90% confidence level obtained for the range $-0.8 \leq \kappa \leq +0.65$. In conclusion, CSV effects that are in reasonably good agreement with high energy data are substantially larger than predicted by theory; valence CSV effects could be four times as large as predicted by Sather and Rodionov or three times as large with opposite sign. For NuTeV measurements, the value $\kappa = -0.6$ would completely remove the anomaly, while the value $\kappa = +0.6$ would double the discrepancy. Note that these two values are within the 90% confidence level limit found by MRST. A recent work by J. T Londergan and A. W. Thomas [9] taking into account the MRST phenomenological analysis showed that the CSV effects are one viable explanation of the anomalous value of the Weinberg angle obtained in the NuTeV experiment. They strongly encouraged experimental investigations to directly measure CSV which can be surprisingly as large as the values obtained by MRST phenomenological fit.

V. FACTORIZATION AT A 12 GEV JLAB

As all semi-inclusive analyses, the formalism used to extract charge symmetry violating quark distributions involves the assumption of factorization, i.e., that semi-inclusive pion production can be described by two independent processes. First, the virtual photon interacts with a quark in the hadronic system - then that quark subsequently hadronizes forming a pion or other particle. Only when this picture is valid can we be confident that the formalism we are using to measure CSV effects is appropriate.

It is not a foregone conclusion that semi-inclusive processes at a 12 GeV JLab will satisfy the factorization criteria described above, however there is good reason to believe that it may. Already at 6 GeV, we have seen signs that factorization may be satisfied. Figs. 1 and 2 show results from Hall C experiment E-00-108 [17] in which semi–inclusive charged pion production from hydrogen and deuterium targets was measured. In this experiment, the absolute cross sections were found to be consistent with cross section calculations performed in a leading order framework using CTEQ5M [18] parton distribution functions and a high energy parameterization of the fragmentation functions [11] (see Fig. 1). In addition, the

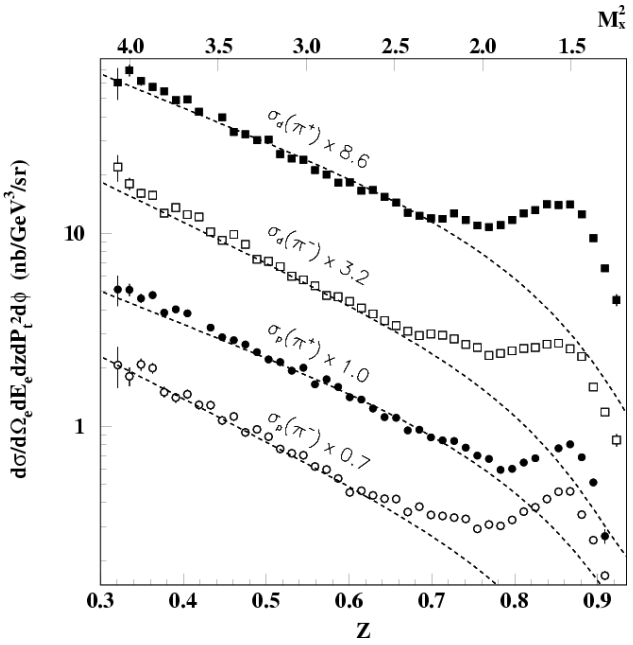

FIG. 1: Cross sections for $H, D(e, e'\pi^{\pm})$ from Hall C experiment E-00-108. Curves denote calculations using a simple factorization picture as described in the text. Closed symbols have been corrected for backgrounds from exclusive ρ production.

z dependence of combinations of the two charge states and targets was also examined. If factorization holds, then the following relations should hold true, independent of z:

$$\frac{\sigma_p(\pi^+) + \sigma_p(\pi^-)}{\sigma_d(\pi^+) + \sigma_d(\pi^-)} = \frac{4u(x) + 4\overline{u}(x) + d(x) + \overline{d}(x)}{5[u(x) + d(x) + \overline{u}(x) + \overline{d}(x)]} \tag{1}$$

and

$$\frac{\sigma_p(\pi^+) - \sigma_p(\pi^-)}{\sigma_d(\pi^+) - \sigma_d(\pi^-)} = \frac{4u_v(x) - d_v(x)}{3[u_v(x) + d_v(x)]}. \tag{2}$$

These ratios are plotted in Fig. 2 and are found to be consistent with the simple factorization assumption up to $z \approx 0.7$.

While the Hall C 6 GeV results are promising, it is important to test for factorization over a wider kinematic range, and especially at the kinematics relevant to the experiment. We plan to perform similar to tests to those performed in E-00-108 to verify that factorization is satisfied at the kinematics sampled by this experiment.

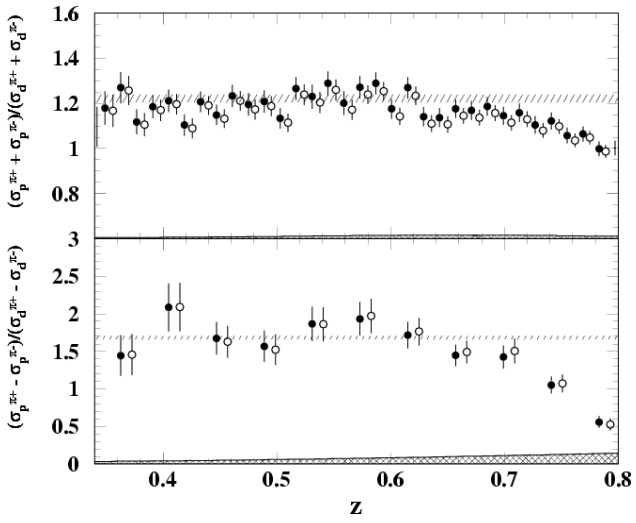

FIG. 2: Ratio of proton to deuterium results for the sum (top) and difference (bottom) of the π^+ and π^- cross sections. The ratios are independent of z up to $z \approx 0.7$.

VI. FORMALISM

Semi-inclusive pion production from lepton deep inelastic scattering on nuclear targets was suggested [4, 16] as a sensitive probe of CSV effects in nucleon valence distributions. The authors proposed measuring the quantity $R^D_{meas}(x,z)$ defined by:

$$R^D_{meas}(x,z) = \frac{4N^{D\pi^-}(x,z) - N^{D\pi^+}(x,z)}{N^{D\pi^+}(x,z) - N^{D\pi^-}(x,z)}, \tag{3}$$

where $N^{D\pi^+}$ ($N^{D\pi^-}$) is the yield of π^+ (π^-) produced in coincidence with the scattered electron from deuterium.

In the quark-parton formalism, the semi-inclusive production of hadrons in DIS from a nucleon is given by:

$$\frac{1}{\sigma_N(x)}\frac{d\sigma^h_N(x,z)}{dz} = \frac{\sum_i e_i^2 q_i^N(x) D_i^h(z)}{\sum_i e_i^2 q_i^N(x)} \tag{4}$$

$q_i^N(x)$ is the distribution function for quarks of flavor i, and charge e_i, in the nucleon N as a function of Bjorken x. $D_i^h(z)$ is the fragmentation function for a quark of flavor i into a hadron h. The fragmentation function depends on the quark longitudinal momentum fraction $z = E_h/\nu$, where E_h is the energy of the hadron and ν is the energy of the virtual photon. The yield of hadron h per scattering from nucleon N can be written as $N^{Nh} = \sum_i e_i^2 q_i^N(x) D_i^h(z)$. In terms of these quantities, semi-inclusive production of a charged pion from a proton

(neutron) can be described by

$$\begin{aligned} N^{p\pm}(x,z) &= \frac{4}{9}u^p(x)D_u^{\pm}(z) + \frac{4}{9}\bar{u}^p(x)D_{\bar{u}}^{\pm}(z) \\ &+ \frac{1}{9}d^p(x)D_d^{\pm}(z) + \frac{1}{9}\bar{d}^p(x)D_{\bar{d}}^{\pm}(z) \\ &+ \frac{1}{9}s^p(x)D_s^{\pm}(z) + \frac{1}{9}\bar{s}^p(x)D_{\bar{s}}^{\pm}(z), \end{aligned} \tag{5}$$

$$\begin{aligned} N^{n\pm}(x,z) &= \frac{4}{9}u^n(x)D_u^{\pm}(z) + \frac{4}{9}\bar{u}^n(x)D_{\bar{u}}^{\pm}(z) \\ &+ \frac{1}{9}d^n(x)D_d^{\pm}(z) + \frac{1}{9}\bar{d}^n(x)D_{\bar{d}}^{\pm}(z) \\ &+ \frac{1}{9}s^n(x)D_s^{\pm}(z) + \frac{1}{9}\bar{s}^n(x)D_{\bar{s}}^{\pm}(z) \end{aligned} \tag{6}$$

Charge Conjugation invariance implies that $D_u^{\pm} = D_{\bar{u}}^{\mp}$ and $D_d^{\pm} = D_{\bar{d}}^{\mp}$. By making the additional assumption of charge symmetry, the fragmentation functions will obey the relations:

$$\begin{aligned} D_d^{\pi^-}(z) &= D_u^{\pi^+}(z) \\ D_d^{\pi^+}(z) &= D_u^{\pi^-}(z), \end{aligned} \tag{7}$$

and the parton distribution functions will satisfy the relations:

$$\begin{aligned} u^p(x) &= d^n(x) \\ d^p(x) &= u^n(x) \end{aligned} \tag{8}$$

Using Eqs (3), (4), (5) and (6), one can derive the expression for R_{meas}^D

$$\begin{aligned} R_{meas}^D(x,z) &= \frac{5\Delta(z)}{1-\Delta(z)} + 5\left[\frac{1+\Delta(z)}{1-\Delta(z)}\right] \times \frac{[\bar{u}^p(x)+\bar{d}^p(x)]}{[u_v^p(x)+d_v^p(x)]} \\ &+ \left[\frac{\Delta_s(z)}{1-\Delta(z)}\right] \frac{[s(x)+\bar{s}(x)]}{[u_v^p(x)+d_v^p(x)]}, \end{aligned} \tag{9}$$

where

$$\Delta(z) = \frac{D_u^{\pi^-}(z)}{D_u^{\pi^+}(z)}, \tag{10}$$

and the strange-favored ratio of the quark fragmentation functions

$$\Delta_s(z) = \frac{D_s^{\pi^+}(z) + D_s^{\pi^-}(z)}{D_u^{\pi^+}(z)} \tag{11}$$

In Eq. (7), we assume the validity of the impulse approximation, *i.e.*,

$$N^{D\pi^{\pm}}(x,z) = N^{p\pi^{\pm}}(x,z) + N^{n\pi^{\pm}}(x,z) \tag{12}$$

In Eq. (7), charge symmetry was also assumed in PDFs and fragmentation functions. Keeping charge-symmetry-violating functions, the $R^D_{meas}(x,z)$ ratio becomes:

$$\begin{aligned} R^D_{meas}(x,z) &= \frac{5\Delta(z)}{1-\Delta(z)} - \frac{[4+\Delta(z)]\delta D(z)}{3[1-\Delta(z)]^2} \\ &+ \left[\frac{1+\Delta(z)}{1-\Delta(z)}\right] \times \left[\frac{4[\delta d(x) - \delta u(x)] + 15[\bar{u}^p(x) + \bar{d}^p(x)]}{3[u^p_v(x) + d^p_v(x)]}\right] \\ &+ \left[\frac{\Delta_s(z)}{1-\Delta(z)}\right] \frac{[s(x)+\bar{s}(x)]}{[u^p_v(x)+d^p_v(x)]} \end{aligned} \tag{13}$$

The quantity R^D_{meas} in Eq. (11) contains the charge-symmetry-violating quark distribution functions

$$\begin{aligned} \delta d(x) &= d^p(x) - u^n(x) \\ \delta u(x) &= u^p(x) - d^n(x), \end{aligned} \tag{14}$$

and the charge symmetry-breaking fragmentation functions

$$\delta D(z) = \frac{D^{\pi^+}_u(z) - D^{\pi^-}_d(z)}{D^{\pi^+}_u(z)} \tag{15}$$

A more clean separation of the x and z dependence can be obtained by multiplying R^D_{meas} by a z-dependent factor, e.g.

$$\tilde{R}^D(x,z) = R^D_f(z) + R^D_{CSV}(x) + R^D_{sea}(x,z) \tag{16}$$

where

$$\begin{aligned} \tilde{R}^D(x,z) &= \frac{1-\Delta(z)}{1+\Delta(z)} R^D_{meas}(x,z), \\ R^D_f(z) &= \frac{5\Delta(z)}{1+\Delta(z)} - \frac{[4+\Delta(z)]\delta D(z)}{3[1-\Delta^2(z)]}, \\ R^D_{CSV}(x) &= \frac{4[\delta d(x) - \delta u(x)]}{3[u^p_v(x) + d^p_v(x)]}, \\ R^D_{sea}(x,z) &= \frac{5[\bar{u}^p(x) + \bar{d}^p(x)] + \Delta_s(z)[s(x)+\bar{s}(x)]/[1+\Delta(z)]}{[u^p_v(x)+d^p_v(x)]} \end{aligned} \tag{17}$$

Equation (11) was obtained by expanding to first order the small quantities which are $\delta d(x)$, $\delta u(x)$, $\delta D(z)$ and the sea quark distribution. Therefore we need to be in the high x region where the ratio of sea to valence quark distributions is small. The quantity $\tilde{R}^D(x,z)$ separates into three pieces. The first piece $R^D_f(z)$ depends only on z. It contains a small part which is proportional to the CSV part of the fragmentation function. The dominant piece of $R^D_f(z)$ has the form $5\Delta(z)/(1+\Delta(z))$. The second term $R^D_{CSV}(x)$ depends only on x, and is proportional to the nucleon CSV term. $R^D_{sea}(x,z)$ is proportional to the sea quark

distributions and can be written as a sum of a strange sea term $R^D_{sea\_S}$ and a non strange sea term $R^D_{sea\_NS}$, where

$$R^D_{sea\_S}(x,z) = \frac{\Delta_s(z)[s(x)+\bar{s}(x)]/[1+\Delta(z)]}{[u^p_v(x)+d^p_v(x)]} \tag{18}$$

$$R^D_{sea\_NS}(x) = \frac{5[\bar{u}^p(x)+\bar{d}^p(x)]}{[u^p_v(x)+d^p_v(x)]} \tag{19}$$

Experimentally, one needs to measure accurately the x dependence of $\tilde{R}^D(x,z)$ for fixed z values. The sea quark distribution should fall off monotonically and rapidly with x. So, if one goes to sufficiently large x, the sea quark contribution will be negligible relative to the CSV term. The CSV contribution of the fragmentation function to the z-dependent term $R^D_f(z)$ was estimated [16] to be 1%. Therefore it can be neglected in the expression of $R^D_f(z)$ which becomes

$$R^D_f(z) \cong \frac{5\Delta(z)}{1+\Delta(z)} \tag{20}$$

By rearranging eq. (14), one obtains the following equation:

$$D(z)\ R(x,z) + CSV(x) = B(x,z) \tag{21}$$

where

$$\begin{aligned} D(z) &= \frac{1-\Delta(z)}{1+\Delta(z)}, \\ R(x,z) &= \frac{5}{2} + R^D_{meas}, \\ CSV(x) &= \frac{-4(\delta d - \delta u)}{3(u_v+d_v)}, \\ B(x,z) &= \frac{5}{2} + R^D_{sea\_S}(x,z) + R^D_{sea\_NS}(x) \end{aligned} \tag{22}$$

In the proposed measurements, we would like to measure $R^D_{meas}(x,z)$ (see Eq. (1)) and thus $R(x,z)$ for 16 bins in x and z for 3 distinct Q^2 bins. We will end up with 16 equations similar to Eq. (13) and 8 unknowns, which are CSV(x_1), CSV(x_2), CSV(x_3), CSV(x_4), D(z_1), D(z_2), D(z_3) and D(z_4). $B(x,z)$ can be obtained from phenomenological PDFs. The chosen x values for the measurements will be best where $R^D_{sea\_S}$ becomes small.

For a better idea about $B(x,z)$ term, we used the PDFs from CTEQ6L and fragmentation functions from a recent parameterization by De Florian and collaborators [19]. Figure 3 shows the contributions of different sea terms. The non strange sea term of Eq. (17) is large compared to the strange term. By choosing x values above 0.35, the strange contribution becomes negligible. Therefore, making the $B(x,z)$ independent of z variable. The $R^D_{sea\_NS}$ term can be obtained from the parton distribution function. The uncertainties on this non strange sea term represent the main theoretical systematical uncertainties on the extracted CSV term.

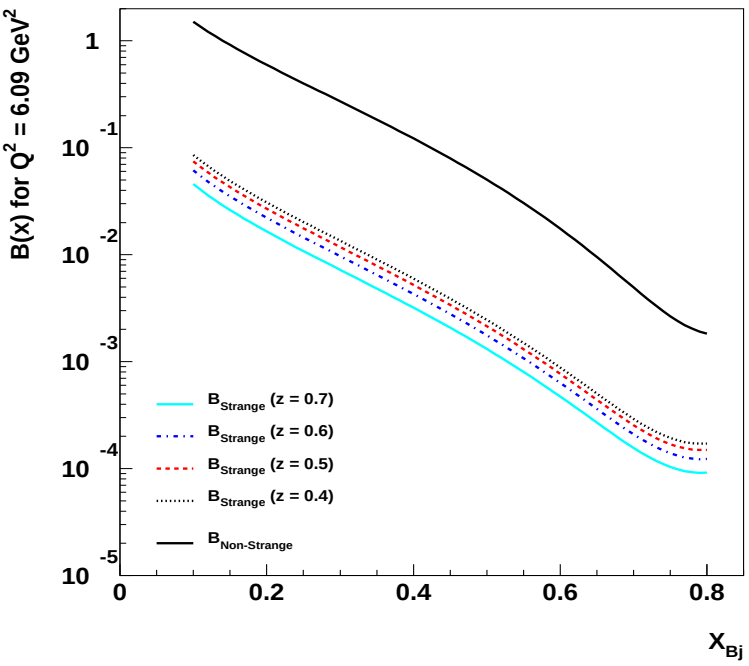

FIG. 3: $B(x, z)$ term as a function of x. The PDFs are taken from CTEQ6L parameterization [18] while fragmentation functions are taken from DSS [19] recent parameterization.

VII. EXPERIMENTAL OVERVIEW

Since the effect we are attempting to measure is potentially small, it is important that systematic errors are well controlled. In particular, since we will be comparing yields of negatively and positively charged pions, it is crucial that the acceptance for the detection of the charged pion is independent of pion charge. For this reason, magnetic, focusing spectrometers hold a clear advantage over large acceptance devices that may have non–charge symmetric acceptance effects. In addition, small angles and large momenta are required, hence Hall C with the HMS and new SHMS are well suited to this experiment.

A. Kinematics

In this experiment we propose to measure the ratio of the π^- to π^+ production yields on deuterium for different x and z bins:

$$R_Y(x, z) = \frac{Y^{\pi-}(x, z)}{Y^{\pi+}(x, z)}$$

This experiment will measure semi–inclusive pion electroproduction from deuterium at large

x to map out potential charge symmetry violation in the valence quark distributions. The kinematics were chosen with the following goals:

- Measure semi–inclusive charged pion electroproduction from deuterium at three different Q^2 (3.5, 5.1 and 6.1 GeV^2). At each Q^2 value cover several values of x and z such that one can extract $R^D_{meas}(x,z)$ at each of these points and thereby extract the charge symmetry violating quark distributions and the fragmentation functions.
- At $Q^2 = 3.5$ GeV^2, semi-inclusive yields will be measured for x =0.3, 0.35, 0.4, and 0.45. At each x setting measurements will be performed at $z = 0.4$, 0.5, 0.6 and 0.7
- At $Q^2 = 5.1$ GeV^2, semi-inclusive yields will be measured for $x = 0.45$, 0.5, 0.55, and 0.6. At each x setting measurements will be performed at $z = 0.4$, 0.5, 0.6 and 0.7
- At $Q^2 = 6.1$ GeV^2, semi-inclusive yields will be measured for x =0.5, 0.55, 0.6 and 0.65. At each x setting measurements will be performed at $z = 0.4$, 0.5, 0.6 and 0.7

In addition, to the above criteria, we require the usual "DIS" kinematics such that $Q^2 > 1$ GeV^2 and $W^2 > 4$ GeV^2. Also, we will require $W'^2 = (m_p + \nu - E_\pi)^2 - |\vec{q} - \vec{p}_\pi|^2$, the mass of the unobserved final state , be larger than 2.5 GeV^2. This last constraint is driven by the observation from E00-108 that factorization seems to hold up to $z = 0.7$, or for their kinematics, $W'^2 > 2$ GeV^2.

The experiment will measure $D(e,e'\pi^+)X$, and $D(e,e'\pi^-)X$ using the HMS and SHMS spectrometers in Hall C. Electrons will be detected in the SHMS and the charged pions in the HMS. The proposed kinematics for this experiment are shown in Tables I, II and III. Electron momenta and angles range from 4.5 to 6.8 GeV and 12.50° to 20.21° respectively while pion kinematics require momenta from 1.67 to 4.55 GeV and angles of 10.70° to 19.93°. These requirements are well within the capabilities of the SHMS and HMS. Note that the minimum separation of 17.5° between both spectrometers is always satisfied.

B. Coincidence and Singles Rate Estimates

Rates for the $D(e,e'\pi^+)X$, and $D(e,e'\pi^-)X$ reactions have been estimated using SIMC, the standard Hall C Monte Carlo package. This simulation includes effects from radiative processes, pion decay, multiple scattering, as well as detailed models of the SHMS and HMS acceptances. It should be noted that the SHMS component of SIMC has not yet been updated to reflect the most recent revisions to the SHMS design. In the Monte Carlo, the SHMS has an approximate solid angle of 3.5 msr and momentum bite of 35%, however, the updated design yields a larger solid angle of 5.0 msr with a slightly smaller

x	z	ν (GeV)	W (GeV)	W' (GeV)^2	θ_e (deg)	θ_q (deg)	E_e (GeV)	P_π (GeV)
				$Q^2 = 3.5$				
0.30	0.40	6.300	3.025	2.405	15.05	10.70	4.700	2.516
0.30	0.50	6.300	3.025	2.227	15.05	10.70	4.700	3.147
0.30	0.60	6.300	3.025	2.032	15.05	10.70	4.700	3.777
0.30	0.70	6.300	3.025	1.816	15.05	10.70	4.700	4.408
0.35	0.40	5.400	2.732	2.181	13.78	13.49	5.600	2.156
0.35	0.50	5.400	2.732	2.025	13.78	13.49	5.600	2.696
0.35	0.60	5.400	2.732	1.854	13.78	13.49	5.600	3.237
0.35	0.70	5.400	2.732	1.666	13.78	13.49	5.600	3.777
0.40	0.40	4.700	2.484	1.992	12.95	16.20	6.300	1.875
0.40	0.50	4.700	2.484	1.854	12.95	16.20	6.300	2.346
0.40	0.60	4.700	2.484	1.704	12.95	16.20	6.300	2.817
0.40	0.70	4.700	2.484	1.538	12.95	16.20	6.300	3.287
0.45	0.40	4.200	2.283	1.839	12.50	18.65	6.800	1.674
0.45	0.50	4.200	2.283	1.715	12.50	18.65	6.800	2.095
0.45	0.60	4.200	2.283	1.581	12.50	18.65	6.800	2.516
0.45	0.70	4.200	2.283	1.434	12.50	18.65	6.800	2.937

TABLE I: Kinematics proposed for this measurement at $Q^2 = 3.5$ GeV^2.

momentum bite of 32%. For our rate estimates, we take the nominal SIMC yield and scale by $5/3.5 \times 32/35 = 1.3$ to account for the new SHMS design.

The model used for the semi-inclusive process combines MRST01-LO parton distributions and Nuclear PDFs of Ref. [20], with fragmentation functions from Refs. [11] and [21].

Coincidence yields are for a 10 cm long liquid deuterium target. Additional data for factorization tests will be taken at $x = 0.3$ and $x = 0.5$ using a 10 cm hydrogen target.

At each setting, care has been taken to keep the total particle yield (including singles rates) in the hadron arm the same for both π^+ and π^- running. This helps reduce the systematic error associated with rate dependent effects in the particle tracking efficiency, as well as potential rate dependent effects in other detectors.

Singles rates for hadrons ($\pi^\pm$,$K^\pm$, and protons) produced from the liquid deuterium target

x	z	ν (GeV)	W (GeV)	W' (GeV)^2	θ_e (deg)	θ_q (deg)	E_e (GeV)	P_π (GeV)
				$Q^2 = 5.1$				
0.45	0.40	6.000	2.659	2.120	17.46	13.54	5.000	2.396
0.45	0.50	6.000	2.659	1.967	17.46	13.54	5.000	2.997
0.45	0.60	6.000	2.659	1.800	17.46	13.54	5.000	3.597
0.45	0.70	6.000	2.659	1.616	17.46	13.54	5.000	4.198
0.50	0.40	5.400	2.438	1.951	16.49	15.76	5.600	2.156
0.50	0.50	5.400	2.438	1.813	16.49	15.76	5.600	2.696
0.50	0.60	5.400	2.438	1.664	16.49	15.76	5.600	3.237
0.50	0.70	5.400	2.438	1.499	16.49	15.76	5.600	3.777
0.55	0.40	4.900	2.240	1.798	15.78	17.92	6.100	1.955
0.55	0.50	4.900	2.240	1.675	15.78	17.92	6.100	2.446
0.55	0.60	4.900	2.240	1.541	15.78	17.92	6.100	2.937
0.55	0.70	4.900	2.240	1.393	15.78	17.92	6.100	3.427
0.60	0.40	4.500	2.063	1.661	15.30	19.93	6.500	1.795
0.60	0.50	4.500	2.063	1.550	15.30	19.93	6.500	2.246
0.60	0.60	4.500	2.063	1.430	15.30	19.93	6.500	2.696
0.60	0.70	4.500	2.063	1.298	15.30	19.93	6.500	3.147

TABLE II: Kinematics proposed for this measurement at $Q^2 = 5.1$ GeV^2.

have been estimated using the parameterization from Wiser [22]. Electron rates have been calculated using a fit to SLAC proton and deuterium data. In general, the singles rates in the hadron arm (the HMS) are rather high, and in particular, are about a factor of two large for positive polarity as compared to negative polarity. In order to minimize the difference between rate dependent inefficiencies (the primary one being the tracking efficiency), we assume that the positive polarity running will be at half the current as the negative polarity running.

In general we assume 50 μA beam current at negative polarity, so the positive polarity running will be at 25 μA. At the kinematic settings where the singles rates exceed 1 MHz for these nominal currents, the beam current is further reduced to 30 μA and 15 μA for negative and positive polarity respectively (accounted for in the beam time table VIII). Singles rates in the HMS are shown in Tables XII, XIII, and XIV and in the SHMS are shown in TableXV and the coincidence rates are shown in Tables IV and V.

x	z	ν (GeV)	W (GeV)	W' (GeV)^2	θ_e (deg)	θ_q (deg)	E_e (GeV)	P_π (GeV)
				$Q^2 = 6.1$				
0.50	0.40	6.500	2.641	2.103	20.21	12.92	4.500	2.596
0.50	0.50	6.500	2.641	1.950	20.21	12.92	4.500	3.247
0.50	0.60	6.500	2.641	1.783	20.21	12.92	4.500	3.898
0.50	0.70	6.500	2.641	1.598	20.21	12.92	4.500	4.548
0.55	0.40	5.900	2.421	1.933	18.96	15.02	5.100	2.356
0.55	0.50	5.900	2.421	1.796	18.96	15.02	5.100	2.947
0.55	0.60	5.900	2.421	1.646	18.96	15.02	5.100	3.537
0.55	0.70	5.900	2.421	1.480	18.96	15.02	5.100	4.128
0.60	0.40	5.400	2.221	1.778	18.07	17.02	5.600	2.156
0.60	0.50	5.400	2.221	1.655	18.07	17.02	5.600	2.696
0.60	0.60	5.400	2.221	1.521	18.07	17.02	5.600	3.237
0.60	0.70	5.400	2.221	1.372	18.07	17.02	5.600	3.777
0.65	0.40	5.000	2.040	1.638	17.48	18.86	6.000	1.995
0.65	0.50	5.000	2.040	1.527	17.48	18.86	6.000	2.496
0.65	0.60	5.000	2.040	1.406	17.48	18.86	6.000	2.997
0.65	0.70	5.000	2.040	1.273	17.48	18.86	6.000	3.497

TABLE III: Kinematics proposed for this measurement at $Q^2 = 6.1$ GeV^2.

C. Particle Identification

This experiment has relatively modest particle identification requirements which should be easily achievable using the standard detectors in the HMS and SHMS spectrometers.

We will be detecting electrons with momenta ranging from 4.5 to 6.8 GeV in the SHMS. The SHMS has available a lead-glass calorimeter, a heavy-gas Čerenkov detector (intended primarily for pion detection, however it can be configured for modest pion rejection at these momenta), and an atmospheric Čerenkov detector (see Fig. 4). We estimate that the π^- rates will be relatively modest (10's of kHz), so pion rejection will not be too difficult. The planned lead-glass calorimeter for the SHMS will have $> 99\%$ electron detection efficiency with $\approx$200:1 pion rejection [23] is almost sufficient for our purposes on its own. However, we will also make use of the heavy gas Čerenkov operated at $<$ 1atm to further reduce the pion background.

x	z	$Q^2(GeV)^2$	π^+(Hz)	π^-(Hz)
0.30	0.40	3.50	14.26	19.10
0.30	0.50	3.50	15.84	19.84
0.30	0.60	3.50	15.43	18.13
0.30	0.70	3.50	12.47	13.84
0.35	0.40	3.50	14.40	19.13
0.35	0.50	3.50	16.76	20.81
0.35	0.60	3.50	16.37	19.07
0.35	0.70	3.50	13.26	14.62
0.40	0.40	3.50	12.81	17.07
0.40	0.50	3.50	14.87	18.46
0.40	0.60	3.50	15.10	17.60
0.40	0.70	3.50	12.73	14.02
0.45	0.40	3.50	9.92	13.29
0.45	0.50	3.50	11.86	14.80
0.45	0.60	3.50	12.20	14.29
0.45	0.70	3.50	11.00	12.15
0.45	0.40	5.10	3.72	4.91
0.45	0.50	5.10	4.15	5.10
0.45	0.60	5.10	3.93	4.51
0.45	0.70	5.10	3.21	3.47
0.50	0.40	5.10	3.08	4.08
0.50	0.50	5.10	3.61	4.45
0.50	0.60	5.10	3.47	4.00
0.50	0.70	5.10	2.91	3.15
0.55	0.40	5.10	2.40	3.19
0.55	0.50	5.10	2.90	3.59
0.55	0.60	5.10	2.88	3.34
0.55	0.70	5.10	2.46	2.68
0.60	0.40	5.10	1.78	2.39
0.60	0.50	5.10	2.11	2.63
0.60	0.60	5.10	2.13	2.48
0.60	0.70	5.10	1.89	2.08

TABLE IV: Coincidence rates from a 10 cm deuterium target. π^- rates are for 50 μA and π^+ are at 25 μA for $Q^2 = 3.5$ GeV^2 and $Q^2 = 5.1$ GeV^2.

x	z	$Q^2(GeV)^2$	π^+(Hz)	π^-(Hz)
0.50	0.40	6.10	1.57	2.07
0.50	0.50	6.10	1.74	2.14
0.50	0.60	6.10	1.65	1.88
0.50	0.70	6.10	1.35	1.45
0.55	0.40	6.10	1.36	1.80
0.55	0.50	6.10	1.52	1.87
0.55	0.60	6.10	1.46	1.67
0.55	0.70	6.10	1.23	1.32
0.60	0.40	6.10	1.06	1.40
0.60	0.50	6.10	1.23	1.52
0.60	0.60	6.10	1.21	1.39
0.60	0.70	6.10	1.03	1.12
0.65	0.40	6.10	0.76	1.01
0.65	0.50	6.10	0.87	1.08
0.65	0.60	6.10	0.88	1.03
0.65	0.70	6.10	0.78	0.85

TABLE V: Coincidence rates from a 10 cm deuterium target. π^- rates are for 50 μA and π^+ are at 25 μA $Q^2 = 6.1$ GeV^2.

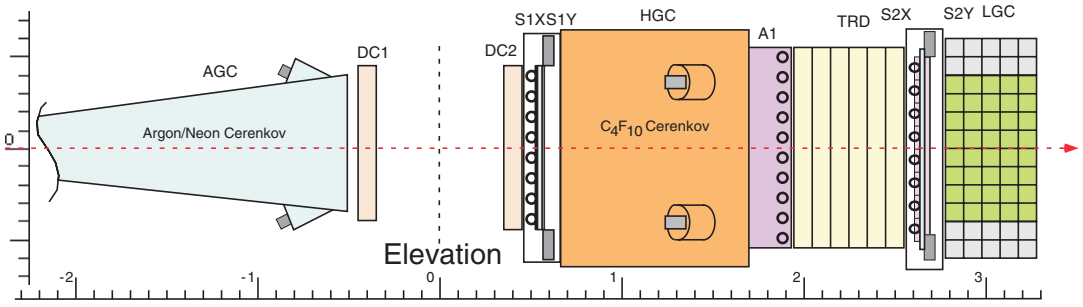

FIG. 4: Schematic of the planned detector stack in the SHMS. An optional Argon-Neon Čerenkov placed before the drift chambers will not be used for this experiment since the lead–glass calorimeter and heavy gas Čereknov will be sufficient to reject the relatively modest rate of charged pions in the SHMS.

The produced pions will be detected in the HMS with momenta ranging from 1.7 to 4.6 GeV. This momentum range is similar to that for Hall C Experiment E-01-107 [24, 25]. In that case, pions were identified using a combination of gas Čerenkov and aerogel detectors. The HMS gas Čerenkov contained C_4F_{10} at a pressure of 0.96 atm. This yields a pion

threshold of 2.65 GeV (kaon threshold of 9.4 GeV) so can reliably be used to separate positively charge pions from kaons and protons. At lower momenta, an aerogel with index of refraction $n = 1.015$ was used (pion threshold = 0.8 GeV). Kaon threshold for this detector is 2.85 GeV, hence pions can be cleanly identified over the full range of momenta accessed in this experiment.

When detecting negatively charged pions in the HMS, we must also reject electrons. The HMS calorimeter electron rejection can be as large as 100:1 at 1 GeV and 1000:1 at 2 GeV with a pion detection efficiency larger than 99.5%. This is more than adequate for the maximum 90 kHz electron rates we expect in the HMS.

Schematically, our pion identification strategy can be summarized:

1. $P_{HMS} = 1.67 - 2.62$ GeV: Pions will fire the $n = 1.015$ aerogel. At $P_{HMS} = 2.62$ GeV, the momentum bite of the HMS will accept particles up to ≈ 2.83 GeV, still below kaon threshold (2.85 GeV) for this detector.

2. $P_{HMS} = 2.86 - 4.54$ GeV: Pions will fire the C_4F_{10} gas Čerenkov at 0.96 atm (threshold=2.65 GeV) while kaons will not. Kaons will, however, begin to fire the aerogel detector.

3. Electrons in the HMS at negative polarity will be rejected by the lead-glass calorimeter, aided by the C_4F_{10} gas Čerenkov below central momenta of 2.62 GeV.

Note that a few settings at $P_{HMS} = 2.696$ GeV and $P_{HMS} = 2.817$ GeV fall in the gap where the HMS Čerenkov will begin to fire for pions in part of the acceptance ($\delta > -1.7\%$ at 2.696 GeV and $\delta > -5.9\%$ at 2.817 GeV) while the aerogel will begin to fire for kaons in part of the acceptance ($\delta > 5.7\%$ at 2.696 GeV and $\delta > 1.2\%$ at 2.817 GeV). In this case, if the kaon backgrounds are found to be too large, we can limit the HMS momentum acceptance (on either the high or low end) to ensure clean pion identification.[2]

When detecting negatively charged pions in the HMS, we must also reject electrons. The HMS calorimeter electron rejection can be as large as 100:1 at 1 GeV and 1000:1 at 2 GeV with a pion detection efficiency larger than 99.5%. This is more than adequate for the maximum 90 kHz electron rates we expect in the HMS.

[2] Alternatively, one can operate the HMS Čerenkov at a pressure larger than 1 atm. to lower the pion threshold slightly. While the Čerenkov detector has been designed with this capability in mind, there is a certain degree of incovencience in that the entrance and exit windows of the detector must be removed and flipped.

VIII. ρ AND $N(e,e'\pi^{\pm})N'$ RADIATIVE BACKGROUNDS

In addition to semi-inclusive production of charged pions, pions from the decay of diffractively produced ρ particles and pions produced exclusively at $z = 1$ that "radiate in" to the spectrometer acceptance will also contribute to the measured yield. Our estimate of the contribution of these processes to our measured signal for a representative sample of the kinematics is summarized in Table VI and Figures 5 and 6.

The contribution from diffractive ρ production was estimated using the ρ cross section from PYTHIA [26] modified to agree with HERMES data [27] with additional modifications to agree with recent CLAS data [28] at lower energies. In general, we find that the contribution from diffractive ρ production is not large ($< 10\%$) at $z \approx 0.5$. At the largest z values ($z = 0.7$), however, this fraction can grow to 20%. To estimate the uncertainty on our extracted signal, the ratio of charged pion yields from deuterium, we assume the parameterization of the ρ cross section used in the simulation is accurate to about 20%. The uncertainty on the contribution to the yield of π^+ events from deuterium at $x = 0.3$, $Q^2 = 3.5$ GeV^2, for example, is then 0.54% (at $z = 0.4$) to 1.96% (at $z = 0.7$). However, contribution to this uncertainty to the π^+/π^- ratio is reduced due to the fact that the yield for π^- events from diffractive ρ production should be identical to that from π^+ events. Hence, in the charge ratio, the uncertainty is reduced to 0.22% to 1.19% (for the $x = 0.5$, $Q^2 = 6.1$ GeV^2 setting, the results are similar: 0.19% to 1.05%). Since the ρ contribution at each z is largely coming from a different region of phase space (in terms of the kinematics of the produced ρ), we assume that the uncertainties are largely uncorrelated between z-bins. This results in a total uncertainty of $\approx$0.36% when averaging over all z bins.

The yield of events from the radiative tail from exclusive pion production (i.e. $e + p(n) \rightarrow e' + \pi^{\pm} n(p) + \gamma$) was estimated using radiative effects implemented in the energy peaking approximation in SIMC combined with a fit to exclusive pion electroproduction for W above the resonance region [29, 30] modified to reproduce the general features of the MAID model [31] at lower W. In general, contributions from these events are quite small, never more than 5% at $z = 0.5$, while growing to $\approx$ 7% at the largest z sampled in this experiment.

Although the total contribution to the yield is smaller when compared to that from diffractive ρ production, the net contribution to the uncertainty in the ratio is comparable. If we again assume that the cross section model used to generate the radiated events is good to 20%, then the uncertainty on the contribution to the yield is $\approx$ 0.7% for π^+ and 0.4% for π^- (assuming 3.5% and 2% as representative, "typical" fractions, excluding points at $z = 0.7$). However, these uncertainties are largely uncorrelated between charge states,

			$Y(\rho \to \pi^+\pi^-)/Y(e'\pi X)$		$Y(e'\pi N\gamma)/Y(e'\pi X)$	
x	z	Q^2 (GeV^2)	π^+	π^-	π^+	π^-
0.3	0.4	3.5	0.027	0.039	0.010	0.005
0.3	0.5	3.5	0.042	0.066	0.034	0.022
0.3	0.6	3.5	0.060	0.101	0.027	0.016
0.3	0.7	3.5	0.098	0.176	0.056	0.039
0.5	0.4	6.1	0.021	0.031	0.007	0.003
0.5	0.5	6.1	0.031	0.050	0.043	0.019
0.5	0.6	6.1	0.047	0.082	0.027	0.012
0.5	0.7	6.1	0.074	0.139	0.063	0.030

TABLE VI: Fractional contribution to the yield of semi–inclusive pions produced from deuterium from pions resulting from the decay of diffractively produced rho, and the radiative tail from exclusive pion production.

resulting in an uncertainty of 0.8% for the charge ratio for deuterium. However, as in the case for the diffractive ρ production discussed above, the kinematical region of the exclusive pions radiating into the acceptance will be slightly different in each z bin. Hence, when averaging over z, the uncertainties will be reduced to ≈0.46%. Again, this will be slightly larger if the largest z bin is included.

It should be noted that the uncertainties due to both the diffractive ρ and exclusive pion radiative tails will likely by smaller once data from JLab, both at 6 and 12 GeV, are fully incorporated into the cross section models of these processes. The estimates made here are based on existing parametrizations typically derived from older data.

IX. UNCERTAINTIES AND PROJECTED RESULTS

At each setting, we will take enough statistics to achieve ≈ 1% uncertainties in the charged pion ratio, $R_D^{\pi^+/\pi^-} = (Y_D(\pi^+)/Y_D(\pi^-))$. The backgrounds from random coincidences are significiant at some settings (see Tables XVI, XVII, and XVIII). At larger z, the backgrounds are smaller so will not contribute singificantly to any amplification of the statistical error, however, at lower z conditions are less favorable. For that reason, we will take 20,000 counts at each setting (and polarity) for the $z = 0.6$ and $z = 0.7$ settings, while we will take 30,000 counts at for $z = 0.4$ and $z = 0.5$ settings.

Uncertainties due to backgrounds from diffractive ρ production and the radiative tail of

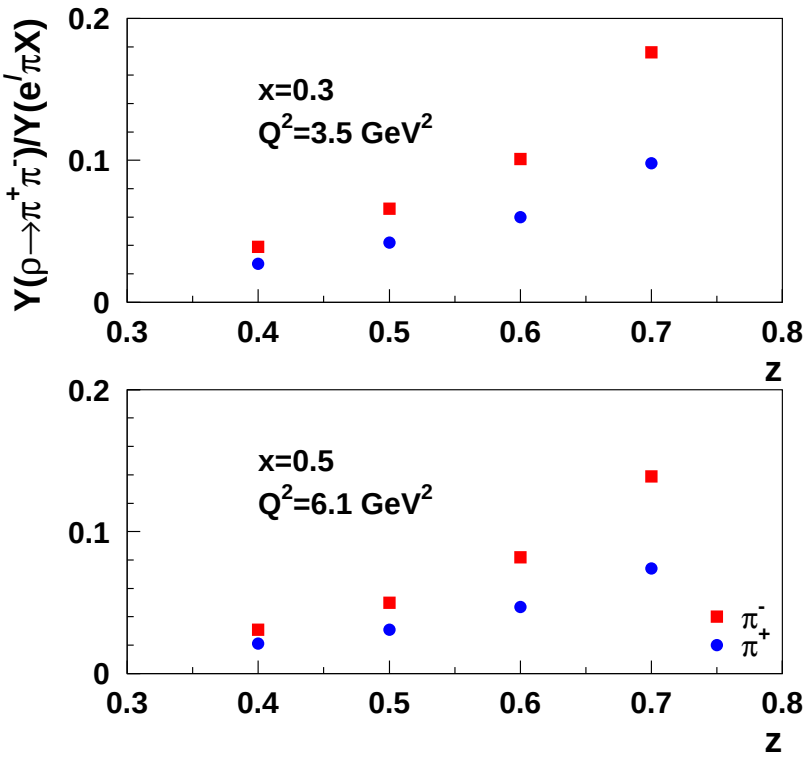

FIG. 5: Contribution of pions coming from the decay of diffractively produced ρ particles to the semi–inclusive yield of π^+ (blue circles) and π^- (red squares) from deuterium plotted as a function of z for two settings. The top panel shows the fraction at $x = 0.3$, $Q^2 = 3.5$ GeV^2 and the bottom panel shows the fraction at $x = 0.5$, $Q^2 = 6.1$ GeV^2 (see Tables I, II and III).

exclusive pion production have already been discussed above and are the largest systematic uncertainties in this experiment. Many experimental systematic uncertainties, such as absolute target thickness completely cancel in the ratio of yields. Others, like pion re-scattering and absorption in the spectrometer, while potentially different for each charge state, are expected to be small. Other notable sources of uncertainty come from the measurement of beam current and boiling effects in the liquid deuterium target. The dominant contribution to the uncertainty in the measurement of the beam current comes from the ≈200 nA noise in the Unser monitor used to calibrate the hall resonating cavity monitors. This leads to a 0.8% (0.4%) uncertainty at 25 μA (50 μA) used for the π^+ (π^-) running. However, this 200 nA is common to both measurements and so only contributes in as much as the current between each charge state is different. Hence the uncertainty on the current measurement in the single target charge ratio is 0.4%. The only remaining uncertainty is then due to the

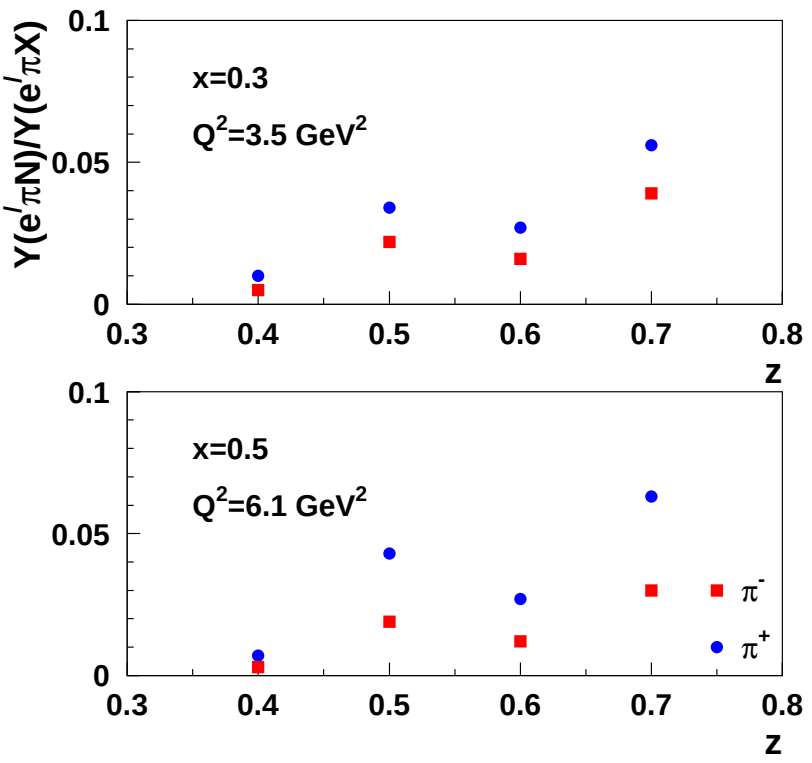

FIG. 6: Contribution from the radiative tail of exclusive pion production to semi-inclusive π^+ (blue circles) and π^- (red squares) production from deuterium plotted as a function of z at two (x,Q^2) settings.

ability to monitor the relative gains of the BCM, which is usually good to 0.1%. Target boiling effects in long cryogenic targets have been observed several times in Hall C. The reduction of luminosity due to these effects varies linearly with beam current. We expect that we will be able to measure this reduction using high–rate inclusive processes to at least 1%. Since the beam currents between pion charge states changes by only a factor of two, this contributes 0.5% to the charge ratio. The (relative) product of the beam charge and target thickness can also be monitored, relying on measurement of the electron singles yields in the SHMS. Since the inclusive electron yield should have high statistics with minimal pion backgrounds, we anticipate the overall normalization uncertainty can be further reduced to 0.2-0.3%.

As discussed earlier, uncertainties due to differences in tracking efficiencies, a potentially large correction at the high single-arm rates of this experiment, will be mitigated by

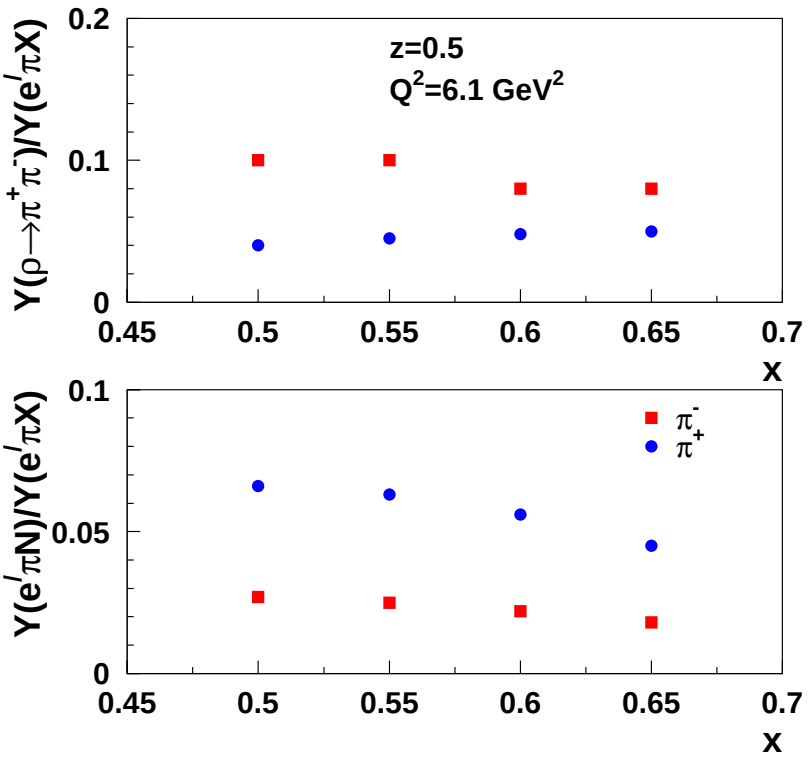

FIG. 7: Contribution from exclusive ρ production (top) and radiative tail of exclusive pion production (bottom) to semi-inclusive π^+ and π^- production from deuterium plotted as a function of x at $Q^2 = 6.1$ GeV^2 and $z = 0.5$.

keeping the singles rates in the hadron arm close to identical. The rates in the electron arm will necessarily be different, but since the global rates are much lower (at most 130 kHz) uncertainties associated with tracking are much smaller.

Other uncertainties due to particle ID efficiency and acceptance should cancel in the ratio, but we include allowance for some small difference, perhaps due to slightly different event distributions across the spectrometer acceptance.

We estimate the total experimental systematic uncertainty in the ratio to be $\Delta R/R = 0.5 - 1.8\%$,varying with z.

Figure 8 shows the expected uncertainties for our measurements of the CSV term which is $(\delta d - \delta u)$. Both statistical and systematical errors are included. The yellow band shows

Source	Uncertainty	Uncertainty in $R_D^{\pi^+/\pi^-}$ (per z bin)
Statistics	0.7%	1.0%
Luminosity	0.3%	0.3%
Tracking efficiency	0.1-1%	0.2%
Dead time	<0.1%	<0.1%
Acceptance	1-2%	0.1%
PID efficiency	<0.5%	0.2%
ρ backgrounds	0.5-3%	0.2-0.7% (1.2%)
Exclusive rad. tail	0.2-1.3%	0.1-0.6% (1.3%)
Total systematic		0.49-1.02% (1.8%)
Total uncertainty	–	1.1-1.43% (2.1%)

TABLE VII: Systematic uncertainties. The uncertainties listed are for *each* z bin so can be combined in quadrature. Numbers in parentheses are for the largest $z = 0.7$ bin, where backgrounds from ρ and the radiative tail from pion electroproduction are larger.

the systematic error related to the parton distribution functions; especially the non strange sea contribution. The expected precision is quite good especially for high x measurements where the magnitude of the non strange sea drops dramatically, making the systematics uncertainties negligible. Since the low x data takes marginally small time, we have decided to extract CSV term for x as low as 0.3 although the systematic errors due to the PDFs are large. One can take a better look at our projections when zooming on the high x region as shown in Figure 9

Using the method described in the formalism section, we will extract simultaneously the x-dependent term related to CSV and the z-dependent term connected to the fragmentation functions. Figure 10 shows the expected uncertainties on this term for different z values. The solid curve is the DSS parameterization.

X. BEAM TIME REQUEST

The required production running time for this experiment is listed in Table VIII and IX. A total of 265 hours is required for data-taking on deuterium. However, about xx hrs of this time is common with the part-II of the this proposal (flavor dependence of the EMC effect). In addition to production data from deuterium, we request $\approx$ 48 hours of data on liquid hydrogen to perform factorization tests at $x = 0.3$ and $x = 0.5$ using the z-scan data. Using this hydrogen data combined with the deuterium data that will be taken at those settings, we will perform tests similar to those done during Hall C experiment E-00-108 (see Figure 2.

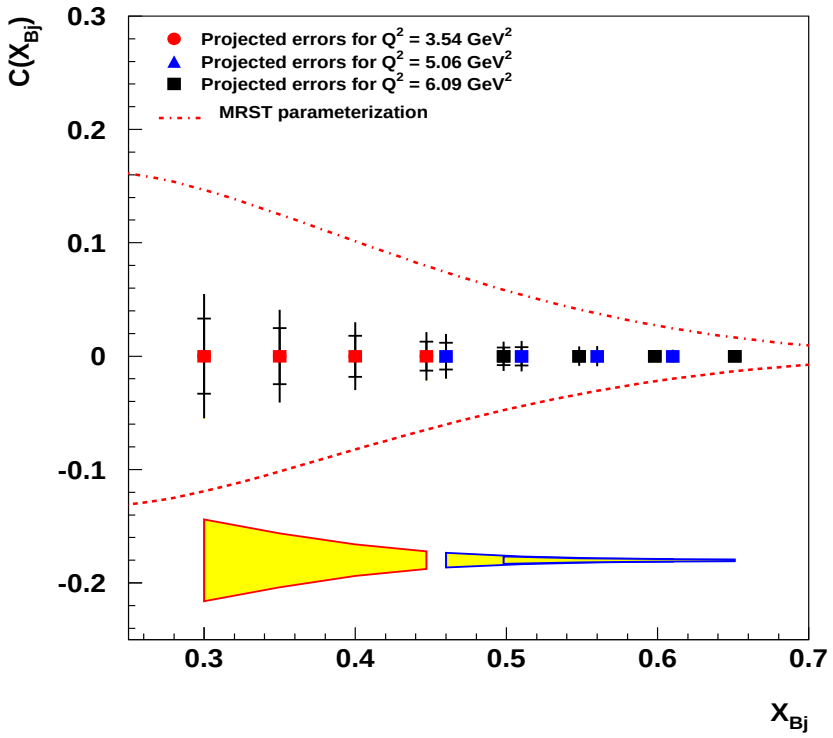

FIG. 8: The two curves are the upper and lower limit of CSV contribution given by MRST parameterization. The dashed curve corresponds to $\kappa = +0.65$ while the dotted-dashed one corresponds to $\kappa = -0.8$. Both statistical and systematical errors are included. The internal errors are statistical uncertainties while the external ones correspond to experimental systematic errors. The yellow band corresponds to the systematic error related to uncertainties in the PDFs.

We also request time for aluminum dummy data taking to subtract contributions from the liquid target cell walls. This is time is shared in common with the part-II of the proposal.

Finally, we allocate 44 hours for various kinematic and polarity changes. At each x point, we plan to minimize systematic effects by taking the z-scan data at one polarity and then changing polarity immediately and completing the setting before moving on to the next x setting. This results in a total of 12 polarity changes at one hour each. In addition, we allocate 20 minutes to each momentum change (48 at each polarity).

We note that if Part I and and Part II of this proposal is approved, the combined running time would be 852 hours, or 35.5 days, 5.5 days shorter than if each were run separately due to the kinematic overlap in the deuterium data–taking.

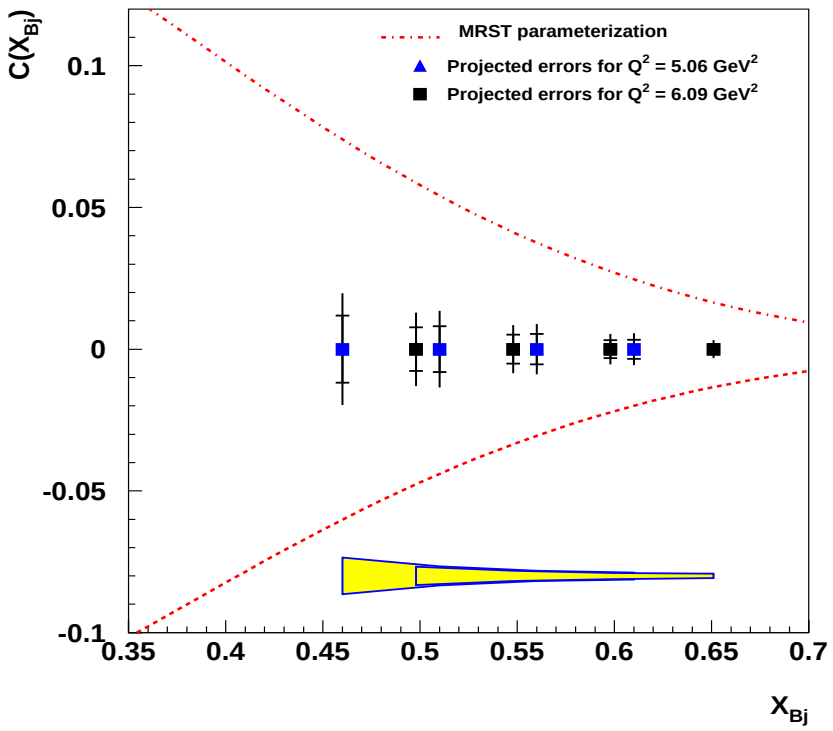

FIG. 9: The two curves are the upper and lower limit of CSV contribution given by MRST parameterization. The dashed curve corresponds to $\kappa = +0.65$ while the dotted-dashed one corresponds to $\kappa = -0.8$. Both statistical and systematical errors are included. The internal errors are statistical uncertainties while the external ones correspond to experimental systematic errors. The yellow band corresponds to the systematic error related to uncertainties in the PDFs.

XI. ACKNOWLEDGEMENTS

The co-spokespersons would like to thank John Arrington, Antje Bruell, and Rolf Ent for helpful discussions and suggestions.

[1] G.A. Miller, B.M.K. Nefkens and I. Slaus, Phys. Rep. 194 (1990) 1

[2] E.M. Henley and G.A. Miller in Mesons in Nuclei, eds. M. Rho and D.H. Wilkinson (North-Holland, Amesterdam 1979)

[3] G.A. Miller, Nucl. Phys. A 518 (1990) 345; I. Slaus, B.M.K. Nefkens and G.A. Miller, Nucl. Inst. and Meth. B 56/57 (1991) 489

[4] J.T. Londergan and A.W. Thomas, Prog. Part. Nucl. Phys. 41 (1998) 49

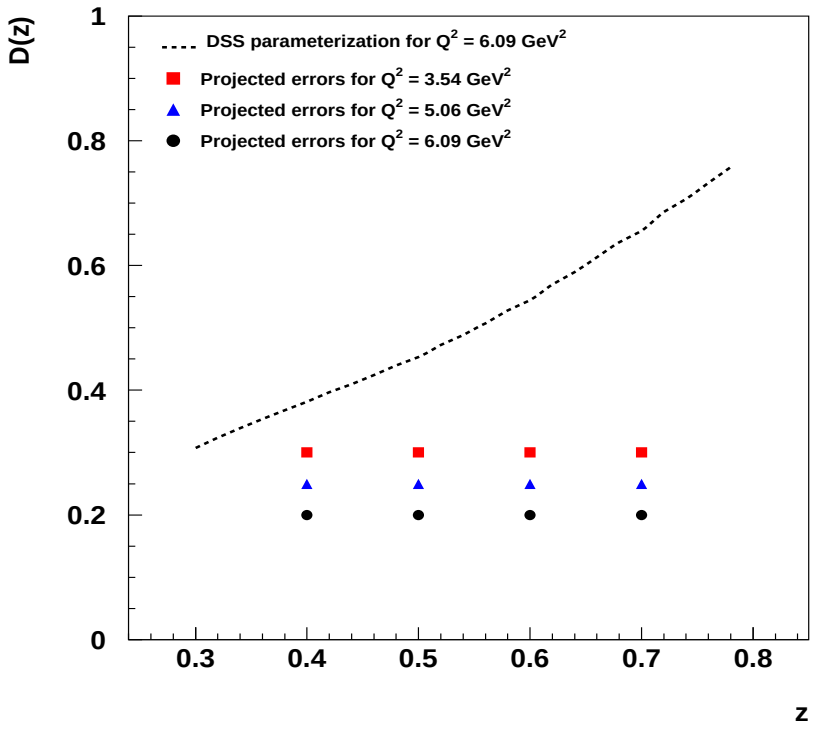

FIG. 10: The solid curve is DSS parameterization. The points reflect the expected uncertainties. Both statistical and systematical errors are included.

[5] P. Amaudruz et al. (NMC Collaboration), Phys. Rev. Lett. 66 (1991) 2712, Phys. Lett. B 295 (1992) 159

[6] A. Baldit et al. (NA51 Collaboration), Phys. Lett. B332 (1994) 244

[7] E.A. Hawker et al, Phys. Rev. Lett. 80 (1998) 3715, R.S. Towell et al., Phys. Rev. D 64 (2001) 052002

[8] G.P. Zeller et al. (NuTeV Collaboration), Phys. Rev. Lett. 88 (2002) 091802

[9] J. T. Londergan and A. W. Thomas, arXiv:hep-ph/0407247.

[10] K. Ackerstaff et al., Phys. Rev. Lett 81 (198) 5519

[11] J. Binnewies, B. A. Kniehl, and G. Kramer, Phys. Rev. D 52 (1995) 4947

[12] W.G. Seligman et al. (CCFR Collaboration), Phys. Rev. Lett. 79 (1997) 1213

[13] E. Sather, Phys. Lett. B 274 (1992) 433

[14] E.N. Rodionov, A.W. Thomas and J.T. Londergan, Mod. Phys. Lett A 9 (1994) 1799

[15] A. D. Martin, R. G. Roberts, W. J. Stirling and R. S. Thorne, Eur. Phys. J. C **35**, 325 (2004) [arXiv:hep-ph/0308087].

[16] J.T. Londergan, A. Pang and A.W. Thomas, Phys. Rev. D 54 (1996) 3154

x	z	$Q^2(GeV^2)$	π^+(hrs)	π^-(hrs)
0.30	0.40	3.50	0.58	0.44
0.30	0.50	3.50	0.53	0.42
0.30	0.60	3.50	0.36	0.31
0.30	0.70	3.50	0.45	0.40
0.35	0.40	3.50	0.58	0.44
0.35	0.50	3.50	0.50	0.40
0.35	0.60	3.50	0.34	0.29
0.35	0.70	3.50	0.42	0.38
0.40	0.40	3.50	0.65	0.49
0.40	0.50	3.50	0.56	0.45
0.40	0.60	3.50	0.37	0.32
0.40	0.70	3.50	0.44	0.40
0.45	0.40	3.50	0.84	0.63
0.45	0.50	3.50	0.70	0.56
0.45	0.60	3.50	0.46	0.39
0.45	0.70	3.50	0.51	0.46
total			145.0	119.8
Grand total				264.9

TABLE VIII: Running time for production data from deuterium targets for $Q^2 = 3.5$ GeV^2. A 10 cm deuterium target is assumed. Times are for 50 μA (25 μA) beam current on target for π^- (π^+) running (except for the first two kinematic points where the current is 30 μA (15 μA). Time estimates for deuterium running assume 20,000 (30,000) counts for $z = 0.6$ and 0.7 ($z = 0.4$ and 0.5) settings for each polarity.

[17] T. Navasardyan *et al.* Phys. Rev. Lett. **98**, 022001, (2007).

[18] J. Pumplin, D. R. Stump, J. Huston, H. L. Lai, P. M. Nadolsky and W. K. Tung, JHEP **0207**, 012 (2002) [arXiv:hep-ph/0201195].

[19] D. de Florian, R. Sassot and M. Stratmann, J. Phys. Conf. Ser. **110**, 022045 (2008) [arXiv:0708.0769 [hep-ph]].

[20] M. Hirai, S. Kumano, T.-H. Nagai, Phys. Rev. C**70** 044905 (2004).

[21] P. Geiger, "Measurement of fragmentation functions at HERMES,"

[22] D. E. Wiser, Ph.D. thesis, Univ. of Wisoconsin (1977).

[23] JLab Experiment 12–06–104, R. Ent and H. Mkrtchyan, spokespersons

[24] JLab Experiment 01–107, D. Dutta, R. Ent, K. Garrow, spokespersons.

[25] B. Clasie *et al.*, Phys. Rev. Lett. **99**, 242502 (2007) [arXiv:0707.1481 [nucl-ex]].

[26] T. Sjostrand, S. Mrenna and P. Skands, JHEP **0605**, 026 (2006) [arXiv:hep-ph/0603175].

x	z	$Q^2(GeV^2)$	π^+(hrs)	π^-(hrs)
0.45	0.40	5.10	2.24	1.70
0.45	0.50	5.10	2.01	1.63
0.45	0.60	5.10	1.41	1.23
0.45	0.70	5.10	1.73	1.60
0.50	0.40	5.10	2.71	2.04
0.50	0.50	5.10	2.31	1.87
0.50	0.60	5.10	1.60	1.39
0.50	0.70	5.10	1.91	1.76
0.55	0.40	5.10	3.47	2.61
0.55	0.50	5.10	2.87	2.32
0.55	0.60	5.10	1.93	1.66
0.55	0.70	5.10	2.26	2.07
0.60	0.40	5.10	4.68	3.49
0.60	0.50	5.10	3.95	3.17
0.60	0.60	5.10	2.61	2.24
0.60	0.70	5.10	2.93	2.68
0.45	0.70	3.50	0.51	0.46
total			145.0	119.8
Grand total				264.9

TABLE IX: Running time for production data from deuterium targets for $Q^2 = 5.1$ GeV^2. A 10 cm deuterium target is assumed. Times are for 50 μA (25 μA) beam current on target for π^- (π^+) running. Time estimates for deuterium running assume 20,000 (30,000) counts for $z = 0.6$ and 0.7 ($z = 0.4$ and 0.5) settings for each polarity

[27] P. Liebing, Ph.D. thesis, Univ. of Hamburg (2004).

[28] C. Hadjidakis, Ph.D. thesis, Institute de Physique Nucleaire d'Orsay (2002).

[29] C. J. Bebek *et al.*, Phys. Rev. D **17**, 1693 (1978).

[30] P. Brauel *et al.*, Z. Phys. C **3**, 101 (1979).

[31] D. Drechsel, S. S. Kamalov, and L. Tiator, Nucl. Phys. **A645**, 145 (1999).

x	z	$Q^2(GeV^2)$	π^+(hrs)	π^-(hrs)
0.50	0.40	6.10	5.31	4.06
0.50	0.50	6.10	4.79	3.89
0.50	0.60	6.10	3.38	2.95
0.50	0.70	6.10	4.13	3.84
0.55	0.40	6.10	6.13	4.63
0.55	0.50	6.10	5.48	4.46
0.55	0.60	6.10	3.81	3.33
0.55	0.70	6.10	4.53	4.20
0.60	0.40	6.10	7.86	5.96
0.60	0.50	6.10	6.78	5.48
0.60	0.60	6.10	4.61	3.99
0.60	0.70	6.10	5.40	4.98
0.65	0.40	6.10	10.96	8.25
0.65	0.50	6.10	9.58	7.716
0.65	0.60	6.10	6.30	5.42
0.65	0.70	6.10	7.14	6.55
0.45	0.70	3.50	0.51	0.46
total			145.0	119.8
Grand total				264.9

TABLE X: Running time for production data from deuterium targets for $Q^2 = 6.1$ GeV^2. A 10 cm deuterium target is assumed. Times are for 50 μA (25 μA) beam current on target for π^- (π^+) running. Time estimates for deuterium running assume 20,000 (30,000) counts for $z = 0.6$ and 0.7 ($z = 0.4$ and 0.5) settings for each polarity

APPENDIX A: APPENDIX I: SINGLES RATES IN THE SHMS AND HMS

In this appendix, we list the expected singles rates in the HMS (hadron arm) and SHMS (electron arm) spectrometers as well as the rates of random coincidences for each setting.

Activity	Time
LD2	264.9
Al. dummy data	26.5
LH2 data	72.1
Polarity and kinematics changes	44
Total	407.5 (17 days)

TABLE XI: Total beam time requested.

			Positive polarity				Negative Polarity			
x	z	ν (GeV)	π^+ (MHz)	K^+ (MHz)	p (MHz)	**Total + (MHz)**	e^- (MHz)	π^- (MHz)	K^- (MHz)	**Total - (MHz)**
0.30	0.40	6.3	0.96	0.16	0.28	**1.40**	0.04	1.25	0.08	**1.37**
0.30	0.50	6.3	0.49	0.10	0.16	**0.75**	0.04	0.66	0.05	**0.76**
0.30	0.60	6.3	0.23	0.06	0.08	**0.37**	0.05	0.32	0.03	**0.40**
0.30	0.70	6.3	0.10	0.03	0.04	**0.18**	0.06	0.15	0.01	**0.22**
0.35	0.40	5.4	0.68	0.11	0.27	**1.06**	0.01	0.88	0.05	**0.95**
0.35	0.50	5.4	0.33	0.07	0.14	**0.55**	0.02	0.45	0.03	**0.50**
0.35	0.60	5.4	0.15	0.04	0.07	**0.26**	0.02	0.21	0.02	**0.25**
0.35	0.70	5.4	0.07	0.02	0.03	**0.12**	0.02	0.09	0.01	**0.12**
0.40	0.40	4.7	0.53	0.08	0.26	**0.86**	0.01	0.67	0.04	**0.72**
0.40	0.50	4.7	0.25	0.05	0.14	**0.43**	0.01	0.33	0.02	**0.36**
0.40	0.60	4.7	0.11	0.03	0.07	**0.20**	0.01	0.15	0.01	**0.17**
0.40	0.70	4.7	0.05	0.01	0.03	**0.09**	0.01	0.07	0.01	**0.08**
0.45	0.40	4.2	0.43	0.06	0.25	**0.74**	0.00	0.54	0.03	**0.57**
0.45	0.50	4.2	0.20	0.04	0.13	**0.37**	0.00	0.26	0.02	**0.28**
0.45	0.50	4.2	0.09	0.02	0.06	**0.17**	0.00	0.12	0.01	**0.13**
0.45	0.60	4.2	0.04	0.01	0.03	**0.07**	0.00	0.05	0.00	**0.06**

TABLE XII: Singles rates in the HMS (hadron arm) at positive and negative polarity from deuterium for $Q^2 = 3.5$ GeV^2 setting. Rates are calculated assuming a 10 cm liquid deuterium target and a beam current of 25 (50) μA a t positive (negative) polarity. Different beam currents are used for the positive and negative polarity to keep the total event rate in the HMS roughly constant between the two polarities.

			Positive polarity				Negative Polarity			
x	z	ν (GeV)	π^+ (MHz)	K^+ (MHz)	p (MHz)	**Total + (MHz)**	e^- (MHz)	π^- (MHz)	K^- (MHz)	**Total - (MHz)**
0.45	0.40	6.0	0.50	0.09	0.20	**0.79**	0.02	0.65	0.04	**0.71**
0.45	0.50	6.0	0.21	0.05	0.10	**0.36**	0.02	0.29	0.02	**0.33**
0.45	0.60	6.0	0.09	0.02	0.04	**0.15**	0.02	0.12	0.01	**0.15**
0.45	0.70	6.0	0.03	0.01	0.02	**0.06**	0.02	0.05	0.00	**0.07**
0.50	0.40	5.4	0.38	0.07	0.19	**0.64**	0.01	0.50	0.03	**0.54**
0.50	0.50	5.4	0.16	0.04	0.09	**0.28**	0.01	0.22	0.02	**0.24**
0.50	0.60	5.4	0.06	0.02	0.04	**0.12**	0.01	0.09	0.01	**0.10**
0.50	0.70	5.4	0.02	0.01	0.01	**0.04**	0.01	0.03	0.00	**0.05**
0.55	0.40	4.9	0.31	0.05	0.18	**0.54**	0.00	0.40	0.02	**0.43**
0.55	0.50	4.9	0.12	0.03	0.08	**0.23**	0.01	0.17	0.01	**0.19**
0.55	0.60	4.9	0.05	0.01	0.03	**0.09**	0.01	0.07	0.01	**0.08**
0.55	0.70	4.9	0.02	0.00	0.01	**0.03**	0.01	0.02	0.00	**0.03**
0.60	0.40	4.5	0.26	0.04	0.18	**0.48**	0.00	0.33	0.02	**0.36**
0.60	0.50	4.5	0.10	0.02	0.08	**0.20**	0.00	0.14	0.01	**0.15**
0.60	0.60	4.5	0.04	0.01	0.03	**0.08**	0.00	0.05	0.00	**0.06**
0.60	0.70	4.5	0.01	0.00	0.01	**0.03**	0.00	0.02	0.00	**0.02**

TABLE XIII: Singles rates in the HMS (hadron arm) at positive and negative polarity from deuterium for $Q^2 = 5.1$ GeV^2 setting. Rates are calculated as described in Fig. XII

			Positive polarity				Negative Polarity			
x	z	ν (GeV)	π^+ (MHz)	K^+ (MHz)	p (MHz)	**Total + (MHz)**	e^- (MHz)	π^- (MHz)	K^- (MHz)	**Total - (MHz)**
0.50	0.40	6.5	0.46	0.09	0.18	**0.72**	0.02	0.61	0.04	**0.67**
0.50	0.50	6.5	0.19	0.05	0.08	**0.31**	0.02	0.26	0.02	**0.30**
0.50	0.60	6.5	0.07	0.02	0.03	**0.13**	0.03	0.10	0.01	**0.14**
0.50	0.70	6.5	0.03	0.01	0.01	**0.05**	0.03	0.04	0.00	**0.07**
0.55	0.40	5.9	0.34	0.06	0.17	**0.57**	0.01	0.46	0.03	**0.50**
0.55	0.50	5.9	0.14	0.03	0.07	**0.24**	0.01	0.19	0.01	**0.21**
0.55	0.60	5.9	0.05	0.01	0.03	**0.09**	0.01	0.07	0.01	**0.09**
0.55	0.70	5.9	0.02	0.01	0.01	**0.03**	0.01	0.02	0.00	**0.04**
0.60	0.40	5.4	0.27	0.05	0.16	**0.48**	0.01	0.36	0.02	**0.39**
0.60	0.50	5.4	0.10	0.02	0.07	**0.19**	0.01	0.14	0.01	**0.16**
0.60	0.60	5.4	0.04	0.01	0.03	**0.07**	0.01	0.05	0.00	**0.06**
0.60	0.70	5.4	0.01	0.00	0.01	**0.02**	0.01	0.02	0.00	**0.03**
0.65	0.40	5.0	0.23	0.04	0.15	**0.42**	0.00	0.30	0.02	**0.32**
0.65	0.50	5.0	0.08	0.02	0.06	**0.17**	0.00	0.11	0.01	**0.13**
0.65	0.60	5.0	0.03	0.01	0.02	**0.06**	0.00	0.04	0.00	**0.05**
0.65	0.70	5.0	0.01	0.00	0.01	**0.02**	0.00	0.01	0.00	**0.02**

TABLE XIV: Singles rates in the HMS (hadron arm) at positive and negative polarity from deuterium for $Q^2 = 6.1$ GeV^2 setting. Rates are calculated as described in Fig. XII

			10 cm LD2			
x	Q^2	ν	π^-	K^-	e	**Total**
	(GeV^2)	(GeV)	(kHz)	(kHz)	(kHz)	**(kHz)**
0.30	3.5	6.3	13.2	1.3	19.8	**34.3**
0.35	3.5	5.4	5.2	0.5	30.7	**36.4**
0.40	3.5	4.7	2.4	0.2	40.9	**43.5**
0.45	3.5	4.2	1.2	0.1	45.9	**47.2**
0.45	5.1	6.0	1.3	0.1	7.1	**8.5**
0.50	5.1	5.4	0.6	0.0	8.5	**9.1**
0.55	5.1	4.9	0.3	0.0	9.3	**9.6**
0.60	5.1	4.5	0.2	0.0	9.4	**9.6**
0.50	6.1	6.5	0.7	0.0	2.8	**3.5**
0.55	6.1	5.9	0.3	0.0	3.3	**3.6**
0.60	6.1	5.4	0.1	0.0	3.6	**3.7**
0.65	6.1	5.0	0.1	0.0	3.6	**3.7**

TABLE XV: Singles rates in the SHMS (electron arm) from a 10 cm deuterium target. The assumed beam current is 50 μA, although the π^+ running will be at only 25 μA. Note that the total rate in the SHMS is low enough (always less than 50 kHz) that uncertainties due to rate dependent efficiency differences should be minimal.

x	z	Q^2 (GeV^2)	I_e (μA)	π (kHz)	e^- (kHz)	Random (Hz)	Real (Hz)	$\frac{Real}{Random}$	I_e (μA)	π (kHz)	e^- (kHz)	Random (Hz)	Real (Hz)	$\frac{Real}{Random}$
			π^+						π^-					
0.30	0.40	3.50	15	579	5.9	6.9	14.3	2.1	30	752	11.9	17.8	19.1	1.1
0.30	0.50	3.50	25	493	9.9	9.8	15.9	1.6	50	664	19.8	26.3	19.8	0.8
0.30	0.60	3.50	25	234	9.9	4.6	15.4	3.3	50	324	19.8	12.8	18.1	1.4
0.30	0.70	3.50	25	105	9.9	2.1	12.5	6.0	50	148	19.8	5.9	13.8	2.4
0.35	0.40	3.50	25	685	15.4	21.0	14.4	0.7	50	884	30.7	54.3	19.1	0.4
0.35	0.50	3.50	25	335	15.4	10.3	16.8	1.6	50	450	30.7	27.6	20.8	0.8
0.35	0.60	3.50	25	153	15.4	4.7	16.4	3.5	50	212	30.7	13.0	19.1	1.5
0.35	0.70	3.50	25	66	15.4	2.0	13.3	6.6	50	94	30.7	5.8	14.6	2.5
0.40	0.40	3.50	25	526	20.4	21.5	12.8	0.6	50	671	40.9	54.9	17.1	0.3
0.40	0.50	3.50	25	249	20.4	10.2	14.9	1.5	50	332	40.9	27.2	18.5	0.7
0.40	0.60	3.50	25	111	20.4	4.5	15.1	3.3	50	153	40.9	12.5	17.6	1.4
0.40	0.70	3.50	25	46	20.4	1.9	12.7	6.7	50	66	40.9	5.4	14.0	2.6
0.45	0.40	3.50	25	428	22.9	19.7	9.9	0.5	50	539	45.9	49.5	13.3	0.3
0.45	0.50	3.50	25	198	22.9	9.1	11.9	1.3	50	261	45.9	24.0	14.8	0.6
0.45	0.70	3.50	25	35	22.9	1.6	11.0	6.9	50	50	45.9	4.6	12.2	2.7

TABLE XVI: Estimate of ratio of real to random coincidences for a 10 cm deuterium target for $Q^2 = 3.5$ GeV^2 setting. Rates are shown for actual currents to be used in data–taking. It is assumed that the singles rates contributing to the random coincidences come from the particle species of interest, i.e. pions in the HMS and electrons in the SHMS. Random coincidence rates are estimated assuming a 2 ns coincidence window. The amplification of the statistical error will be non–trivial due to the significant random backgrounds; for the x-scan data at fixed, the ratio of real to random coincidences is on the order of 1. The real to random ratio for the gold running is not shown, but is similar at each setting.

x	z	Q^2 (GeV^2)	I_e (μA)	π (kHz)	e^- (kHz)	Random (Hz)	Real (Hz)	$\frac{Real}{Random}$	I_e (μA)	π (kHz)	e^- (kHz)	Random (Hz)	Real (Hz)	$\frac{Real}{Random}$
			π^+						π^-					
0.45	0.40	5.10	25	496	3.6	3.5	3.7	1.1	50	653	7.1	9.3	4.9	0.5
0.45	0.50	5.10	25	214	3.6	1.5	4.2	2.7	50	294	7.1	4.2	5.1	1.2
0.45	0.60	5.10	25	86	3.6	0.6	3.9	6.4	50	121	7.1	1.7	4.5	2.6
0.45	0.70	5.10	25	32	3.6	0.2	3.2	14.0	50	47	7.1	0.7	3.5	5.2
0.50	0.40	5.10	25	382	4.2	3.3	3.1	0.9	50	500	8.5	8.5	4.1	0.5
0.50	0.50	5.10	25	159	4.2	1.4	3.6	2.7	50	217	8.5	3.7	4.5	1.2
0.50	0.60	5.10	25	61	4.2	0.5	3.5	6.7	50	87	8.5	1.5	4.0	2.7
0.50	0.70	5.10	25	22	4.2	0.2	2.9	15.4	50	32	8.5	0.6	3.2	5.7
0.55	0.40	5.10	25	308	4.7	2.9	2.4	0.8	50	400	9.3	7.5	3.2	0.4
0.55	0.50	5.10	25	124	4.7	1.2	2.9	2.5	50	169	9.3	3.2	3.6	1.1
0.55	0.60	5.10	25	47	4.7	0.4	2.9	6.6	50	66	9.3	1.2	3.3	2.7
0.55	0.70	5.10	25	16	4.7	0.1	2.5	16.1	50	24	9.3	0.4	2.7	6.0
0.60	0.40	5.10	25	259	4.7	2.4	1.8	0.7	50	333	9.4	6.3	2.4	0.4
0.60	0.50	5.10	25	102	4.7	1.0	2.1	2.2	50	137	9.4	2.6	2.6	1.0
0.60	0.60	5.10	25	37	4.7	0.3	2.1	6.1	50	52	9.4	1.0	2.5	2.5
0.60	0.70	5.10	25	13	4.7	0.1	1.9	15.6	50	19	9.4	0.4	2.1	5.9

TABLE XVII: Estimate of ratio of real to random coincidences for a 10 cm deuterium target for $Q^2 = 5.1$ GeV^2 setting. Rates calculated as described in Table XVI.

x	z	Q^2 (GeV^2)	I_e (μA)	π (kHz)	e^- (kHz)	Random (Hz)	Real (Hz)	$\frac{Real}{Random}$	I_e (μA)	π (kHz)	e^- (kHz)	Random (Hz)	Real (Hz)	$\frac{Real}{Random}$
			π^+						π^-					
0.50	0.40	6.10	25	458	1.4	1.3	1.6	1.2	50	609	2.8	3.4	2.1	0.6
0.50	0.50	6.10	25	188	1.4	0.5	1.7	3.2	50	260	2.8	1.5	2.1	1.5
0.50	0.60	6.10	25	71	1.4	0.2	1.7	8.2	50	102	2.8	0.6	1.9	3.3
0.50	0.70	6.10	25	25	1.4	0.1	1.4	19.0	50	37	2.8	0.2	1.5	7.0
0.55	0.40	6.10	25	344	1.7	1.6	1.4	1.2	50	456	3.3	3.0	1.8	0.6
0.55	0.50	6.10	25	135	1.7	0.5	1.5	3.4	50	187	3.3	1.2	1.9	1.5
0.55	0.60	6.10	25	49	1.7	0.2	1.5	8.9	50	70	3.3	0.5	1.7	3.6
0.55	0.70	6.10	25	17	1.7	0.1	1.2	22.2	50	24	3.3	0.2	1.3	8.1
0.60	0.40	6.10	25	274	1.8	1.0	1.1	1.1	50	360	3.6	2.6	1.4	0.5
0.60	0.50	6.10	25	103	1.8	0.4	1.2	3.3	50	143	3.6	1.0	1.5	1.5
0.60	0.60	6.10	25	36	1.8	0.1	1.2	9.7	50	52	3.6	0.4	1.4	3.7
0.60	0.70	6.10	25	12	1.8	0.0	1.0	24.1	50	17	3.6	0.1	1.1	8.9
0.65	0.40	6.10	25	227	1.8	0.8	0.8	0.9	50	297	3.6	2.1	1.0	0.5
0.65	0.50	6.10	25	83	1.8	0.3	0.9	2.9	50	114	3.6	0.8	1.1	1.3
0.65	0.60	6.10	25	28	1.8	0.1	0.9	8.7	50	40	3.6	0.3	1.0	3.6
0.65	0.70	6.10	25	9	1.8	0.0	0.8	24.3	50	13	3.6	0.1	0.9	9.0

TABLE XVIII: Estimate of ratio of real to random coincidences for a 10 cm deuterium target for $Q^2 = 6.1$ GeV^2 setting. Rates calculated as described in Table XVI.